

**High-Level *Ab Initio* Investigation of the $\text{NH}_2 + \text{O}$ Reaction: Insights into the Potential
Energy Surface and Kinetics**

Ying Xing, Weijie Hua,^{*} and Junxiang Zuo^{*}

MIT Key Laboratory of Semiconductor Microstructure and Quantum Sensing, Department of Applied Physics,
School of Physics, Nanjing University of Science and Technology, Nanjing 210094, China

^{*}Corresponding author: wjhua@njust.edu.cn; jxzuo@njust.edu.cn.

Abstract

The reaction between NH_2 and O represents a critical oxidation pathway in the combustion of ammonia and hydrazine. However, significant discrepancies persist among previous experimental and theoretical studies regarding its kinetics. In this work, we present a high-level theoretical characterization of the NH_2O potential energy surface (PES) using the internally contracted multi-reference configuration interaction (ic-MRCI) method with the cc-pVTZ-F12 basis set. The full-dimensional PES was constructed *via* the permutation invariant polynomial-neural network (PIP-NN) approach, encompassing all energetically accessible channels, including $\text{HNO} + \text{H}$, $\text{NH} + \text{OH}$, $\text{NO} + \text{H}_2$, and $\text{HON} + \text{H}$. Stationary points were characterized with particular attention to the intricate multi-reference nature of the system. Based on the refined PES, we computed thermal rate coefficients and branching ratios over a wide temperature range. Our results provide accurate, first-principles kinetic data that are essential for refining combustion models of nitrogen-containing fuels.

I. Introduction

The prospective utilization of ammonia as a sustainable, carbon-free fuel has garnered significant recent interest, owing to its potential as a hydrogen carrier and its promise in decarbonizing energy systems.¹⁻⁵ The combustion chemistry of ammonia is fundamentally governed by the reactivity of key radical intermediates, among which the amino radical (NH₂) is paramount. In particular, kinetic sensitivity analyses have consistently identified the reaction of NH₂ with ground-state atomic oxygen, O(³P), as a highly sensitive pathway exerting considerable influence on key combustion properties, such as the laminar burning velocity.⁶⁻¹⁰ A precise, quantitative understanding of the elementary reaction mechanisms in ammonia combustion is therefore not only of fundamental interest but is also crucial for optimizing combustion efficiency and advancing related technologies.

The NH₂ + O(³P) reaction proceeds through several energetically accessible product channels:



Despite its critical importance, the kinetics and dynamics of this reaction are not yet fully resolved, especially at high temperatures (>500 K). Early experimental studies, primarily conducted at low temperatures, established that the total rate constant is largely pressure-independent and that the HNO + H channel (R1) dominates, with a minor contribution from the NH + OH channel (R2).¹¹⁻
¹⁴ At room temperature, Dransfield *et al.*¹² reported an overall rate constant of $(8.8 \pm 2.5) \times 10^{-11}$ cm³·molecule⁻¹·s⁻¹ using laser magnetic resonance and laser-induced fluorescence within a flow-tube reactor, which is about 25 times higher than that obtained in earlier flash photolysis study by

Gehring *et al.*¹¹. Meanwhile, the product-specific rate constants for the R1 and R2 channels were quantified via computer modeling of radical concentration profiles as $(7.6\pm 2.0)\times 10^{-11}$ and $(1.2\pm 0.5)\times 10^{-11}$ $\text{cm}^3\cdot\text{molecule}^{-1}\cdot\text{s}^{-1}$, respectively.¹² Adamson *et al.*¹³ proposed that the room-temperature rate constants for the $\text{NH}_2 + \text{O}$ reaction is $(6.5\pm 1.3)\times 10^{-11}$ $\text{cm}^3\cdot\text{molecule}^{-1}\cdot\text{s}^{-1}$ and the branching into channel R2 is only 5-8% by infrared kinetic spectroscopy. Inomata and Washida¹⁴ examined the temperature dependence of the reaction $\text{NH}_2 + \text{O}$ and temperature-independent overall rate constants of $(1.2\pm 0.3)\times 10^{-10}$ $\text{cm}^3\cdot\text{molecule}^{-1}\cdot\text{s}^{-1}$ was observed over the temperature range 242-473 K in a few Torr. Crossed molecule beam scattering experiments reveal that both the OD and HNO products from $\text{ND}_2/\text{NH}_2 + \text{O}(^3\text{P})$ reactions exhibit remarkably cold internal state distributions, indicating a significant exit barrier inconsistent with statistical predictions.^{15, 16} Experimental data at elevated temperatures relevant to combustion is sorely lacking, and significant discrepancies persist among the limited existing studies.

Theoretical efforts to characterize the underlying potential energy surface (PES) of NH_2O system have also been limited. Seminal work by Walch¹⁷ employed complete active space self-consistent field (CASSCF) and internally contracted configuration interaction (ICCI) methods, while Yang *et al.*¹⁸ and Wolf *et al.*¹⁹ applied the Gaussian-2 (G2) methodology to map stationary points. Subsequent kinetic studies, such as those by Bozzelli and Dean²⁰ and Duan *et al.*²¹, have relied on these earlier electronic structure data or simplified theoretical frameworks, inevitably constraining the accuracy of their predictions. Using the CCSD(T)/MP2/6-31G(d,p) level of theory, Sumathi *et al.*²² identified a third reaction channel producing $\text{NO} + \text{H}_2$ (R3) and predicted equal branching ratios for R1, R2, and R3 at room temperature, a finding that conflicts with all existing experimental data. While the broader NH_2O PES has been explored in the context of related reactions (e.g., $\text{H} + \text{HNO}$, $\text{NH} + \text{OH}$, H_2NO decomposition),²²⁻²⁹ the insights from these studies

are inherently limited by the computational methods available at the time, often failing to fully capture the multi-reference character and anharmonic effects critical for this system. In 2014, Homayoon and Bowman³⁰ reported the first global PES for reverse $\text{N}(^2\text{D}) + \text{H}_2\text{O}$ reaction, constructed via a permutationally invariant linear least-squares fit to extensive UCCSD(T)-F12/aug-cc-pVTZ energies (supplemented by some MS-CASPT2 calculations in multireference regions), and used quasi-classical trajectory (QCT) calculations to analyze the internal state distribution of the $\text{NH} + \text{OH}$ channel. Meanwhile, Isegawa *et al.*³¹ carried out a CASPT2-based investigation into the reaction paths of $\text{N}(^2\text{D}) + \text{H}_2\text{O}$ on the two lowest doublet states, specifically focusing on the key roaming pathways. Recently, Klippenstein *et al.*³² recently investigated the NH_2O PES using a high-level CCSD(T)-F12 and ANL1' composite method, and derived the associated kinetics with variable reaction coordinate transition state theory (VRC-TST) alongside master equation simulations. Their findings demonstrate that, under combustion conditions, the $\text{NH}_2 + \text{O}$ reaction primarily proceeds through $\text{HNO} + \text{H}$ and $\text{NH} + \text{OH}$ channels, with a previously overlooked $\text{NO} + \text{H}_2$ pathway contributing about 10% of the total reactive flux.

The development of accurate combustion models for nitrogen-containing fuels is fundamentally hindered by two interrelated limitations: the absence of a high-accuracy, full-dimensional PES for the pivotal NH_2O system, and the consequent lack of rigorous dynamical investigations. Resolving this deficiency is essential for clarifying long-standing kinetic discrepancies and for generating reliable first-principles data under combustion-relevant conditions. To this end, we present a theoretical framework that seamlessly integrates state-of-the-art *ab initio* calculations, machine-learning driven PES construction, and high-throughput QCT simulations. Specifically, the electronic ground state of NH_2O is characterized at the multi-reference configuration interaction (MRCI)^{33, 34} level with large basis set. A global

full-dimensional PES is then constructed by fitting over 62,000 *ab initio* energy points using the permutation-invariant polynomial-neural network (PIP-NN)^{35, 36} approach. This novel PES provides the robust foundation for exhaustive QCT calculations to elucidate the reaction mechanism, quantify accurate thermal rate constants, and determine branching ratios across a wide temperature range. This comprehensive methodology enables us to offer unprecedented insight into the microscopic reaction dynamics of $\text{NH}_2 + \text{O}$ and provide foundational kinetic data essential for refining combustion models of nitrogen-containing fuels.

The remainder of this paper is organized as follows: Section II details the computational methodology, including the *ab initio* calculations, PES construction, and dynamics simulations. The results and a thorough discussion are presented in Section III, and the principal conclusions are summarized in Section IV.

II. Computational Methods

A. *Ab initio* calculations

This study focuses on the ground doublet electronic state ($^2A'$) of the NH_2O system. $\text{NH}_2 + \text{O}$ reaction constitutes a prototypical radical-radical encounter, for which a quantitative assessment of multireference character across different regions of the PES is essential. To this end, we employed the M diagnostic, which is based on natural orbital occupation numbers, to evaluate the extent of strong electronic correlation. The computed M values for all stationary points on the $\text{NH}_2\text{O}(^2A')$ PES are summarized in Table I. These results reveal pronounced multireference character ($M > 0.10$) at every stationary point, confirming the necessity of a multireference treatment for this reaction system. Accordingly, all electronic structure calculations were performed using the dynamically weighted state-averaged complete active space self-consistent field (DW-SA-CASSCF) method^{37, 38}. Specifically, the active space comprised 9 electrons in 8

orbitals, and three-state ($3\ ^2A'$) DW-SA-CASSCF calculations were carried out with the weighting function $w(i) = 1/\cosh^2(\beta\Delta E)$, where $\Delta E = E_i - E_0$ is the energy difference between the i -th state and the ground state, and $\beta^{-1} = 3.0$ eV. The resulting reference wave functions were subsequently employed in explicitly correlated multireference configuration interaction (MRCI-F12)³⁴ calculations, in which higher-order excitation effects and size-extensivity corrections were accounted for via the rotated-reference Davidson (+Q) scheme³⁹. To ensure compatibility with the explicitly correlated formalism and to balance computational cost with accuracy, the correlation-consistent polarized valence triple-zeta basis set designed for F12 methods (cc-pVTZ-F12)⁴⁰ was employed throughout. For comparative validation, the reactants and four products structures were also optimized at the explicitly correlated unrestricted coupled-cluster level with single, double, and perturbative triple excitations (UCCSD(T)-F12)^{41, 42}. All single-point energy calculations required for constructing the global PES were carried out at the MRCI-F12+Q/cc-pVTZ-F12 level of theory using the MOLPRO program package⁴³.

B. Construction of the potential energy surface

The global full-dimensional PES was constructed using the PIP-NN approach, which provides highly accurate representation of PESs with build-in permutation invariance. The fitting database was generated through an initial sampling of relevant configuration space via direct dynamics calculations performed at the UB3LYP/6-311+G(d,p) level. From this initial dataset, representative geometries were selected, and their single-point energies were computed at the high-level MRCI-F12+Q/cc-pVTZ-F12 theory. A preliminary PES was first fitted using the PIP-NN method. Subsequently, an ensemble of quasi-classical trajectories was propagated on this primitive PES to dynamically sample regions critical to the reaction dynamics with initial conditions sampled from thermal distributions of vibrational, rotational, and translational energies. Candidate

geometries were selected based on two criteria: (1) energies below 5 eV relative to the $\text{NH}_2 + \text{O}$ asymptotic limit, and (2) significant deviation among the three best-fitted PESs. To avoid excessive point density across the configuration space, a new geometry was retained only if its Euclidean distance⁴⁴ (in the space of internuclear distances) from all existing points exceeded 0.15 Å. This iterative refinement process resulted in a final database of approximately 62,000 geometries, which was used to obtain the converged global PES.

The permutation symmetry of the two hydrogen atoms was encoded in the PES through a set of 49 permutationally invariant polynomials (PIPs)⁴⁵ up to third-order, which served as the input to the neural network (NN). The PIPs were built from Morse-like variables of the form $p_{ij} = \exp(-r_{ij}/\alpha)$, where r_{ij} denotes the internuclear distance between atoms i and j , and α was set to 1.5 Å. A standard feedforward NN with the architecture 49–30–50–1 (input layer, two hidden layers, output layer) was adopted. The hidden layers employed hyperbolic tangent activation functions, while a linear activation was used in the output layer. The dataset was randomly partitioned into training (90%), validation (5%), and testing (5%) subsets. Network training was conducted using the Levenberg–Marquardt algorithm⁴⁶ in conjunction with “early stopping” criterion⁴⁷ to minimize the root-mean-square error (RMSE), defined as $\text{RMSE} =$

$$\sqrt{\sum_{i=1}^{N_{\text{data}}} (E_i^{\text{PES}} - E_i^{\text{ab initio}})^2 / N_{\text{data}}},$$

where E_i^{PES} and $E_i^{\text{ab initio}}$ denote the fitted and *ab initio* energies of the i -th data point, respectively. This strategy effectively prevents overfitting during the training process. A total of 100 independent neural networks were trained and the final PES was constructed by averaging the predictions of the three best-performing networks in the ensemble, thereby enhancing both robustness and predictive reliability.

C. Quasi-Classical Trajectory Calculations

QCT calculations for the $\text{NH}_2 + \text{O}$ reaction were carried out on the newly developed global PES using the VENUS96 program package.⁴⁸ Trajectories were initiated with a reactant separation of 10.0 Å and terminated when any product fragment reached 15.0 Å or when non-reactive trajectories results in a reactant separation of 15.0 Å. A time step of 0.1 fs was used for numerical integration. The maximum impact parameter, b_{max} , was determined as 8.5 Å based on 10 000 preliminary trajectories at 200 K. To mitigate the inherent zero-point energy (ZPE) leakage issue in QCT simulations, a “passive” ZPE correction scheme⁴⁹ was applied, in which trajectories ending with any reactants or products vibrational mode fell below its corresponding ZPE were excluded from the reactive event count.

The thermal rate constant, $k(T)$, was determined as:

$$k(T) = g_e \left(\frac{8k_B T}{\pi \mu} \right)^{1/2} \pi b_{\text{max}}^2 \frac{N_r}{N_{\text{tot}}}. \quad (1)$$

Here, $\mu = (m_{\text{NH}_2} m_{\text{O}}) / (m_{\text{NH}_2} + m_{\text{O}})$ is the reduced mass of the reactants, k_B is the Boltzmann constant, and N_r and N_{tot} denote the numbers of reactive and total trajectories, respectively. An electronic degeneracy factor⁵⁰ was incorporated to account for the electronic partitions of the reactants and the adiabatic PES:

$$g_e = \frac{q_{\text{NH}_2\text{O}}}{q_{\text{NH}_2} q_{\text{O}}}. \quad (2)$$

The electronic partition functions are: $q_{\text{NH}_2\text{O}} = 2$ for the ${}^2A'$ state; $q_{\text{NH}_2} = 2$ for NH_2 ; and $q_{\text{O}} = 5 + 3e^{-158.5\text{cm}^{-1}/k_B T} + e^{-226.5\text{cm}^{-1}/k_B T}$ for the spin-orbit split triplet $\text{O}({}^3\text{P})$ atom.

The statistical uncertainty is evaluated as $\Delta = [(N_{\text{tot}} - N_r) / (N_{\text{tot}} N_r)]^{1/2}$.

III. Results and Discussion

A. Features of the Potential Energy Surface

The optimized geometries of asymptotes and stationary points, obtained at the MRCI-F12/cc-pVTZ-F12 level, are listed in Table II. Their corresponding relative energies and harmonic vibrational frequencies are summarized in Table III, along with values from our fitted PES, the UCCSD(T)-F12/cc-pVTZ-F12 calculations, and available experimental benchmarks⁵¹. Following ZPE correction, the MRCI-F12-derived reaction energies for the four product channels exhibit significantly better agreement with experiments than the UCCSD(T)-F12 results. The respective deviations from experiments for the HNO + H, NH + OH, NO + H₂ and HON + H channels are 0.13, 0.17, 0, and 0.29 kcal/mol at the MRCI-F12 level, versus 2.71, 0.25, 2.91, and 1.55 kcal/mol at the UCCSD(T)-F12 level. For broader comparison, literature energy benchmarks for stationary points relative to the present MRCI-F12 calculations are displayed in Figure 1. The results clearly indicate a notable sensitivity of stationary-point energetics to the choice of electronic structure theory.

A total of 62,452 *ab initio* points calculated at the MRCI-F12 level were employed in the PIP-NN fit for the multichannel NH₂ + O reaction. The energy distribution of these points is shown in Figure 2(a). The final averaged PES achieves a RMSE of 0.63 kcal/mol and a maximum deviation of 20.21 kcal/mol. The fitting errors for all *ab initio* data and their distribution are presented in Figure 2(b) and 2(c), respectively, demonstrating that the fitted surface reproduces the reference data with high fidelity.

The PES reveals a complex network of isomerization and dissociation pathways. Figure 3 presents a schematic energy diagram of the ground doublet state (²A') PES, showing both *ab initio* and fitted values for the three minima (H₂NO, *trans*-HNOH, and *cis*-HNOH), the five transition states (TS1-TS5), and the four product channels (HNO + H, NH + OH, NO + H₂, and HON + H) relevant to NH₂ + O reactants.

The reaction initiates via the barrierless association of NH_2 and O , forming a deep H_2NO intermediate located 90.28 kcal/mol below the reactant asymptote. This intermediate serves as a common junction for all four reaction channels (R1)-(R4) on the $^2A'$ PES. From H_2NO , several microscopic reaction pathways become accessible. The H_2NO intermediate can isomerize to *trans*- HNOH via TS1 through a 1,2-hydrogen shift, overcoming a barrier of 53.29 kcal/mol relative to H_2NO . Alternatively, it may undergo direct dissociation to $\text{HNO} + \text{H}$ (R1) or $\text{NO} + \text{H}_2$ (R4) over substantially higher barriers of 67.67 kcal/mol (TS5) and 66.73 kcal/mol (TS3), respectively.

The isomerization between *trans*- and *cis*- HNOH proceeds through TS2, located only 13.79 kcal/mol above the *trans* conformer. Both HNOH isomers can further dissociate to common product channels. They may undergo direct cleavage to form $\text{NH} + \text{OH}$ (R2) or $\text{HNO} + \text{H}$ (R4), while hydrogen elimination via TS4 yields $\text{HNO} + \text{H}$ (R1). Notably, all five transition states lie energetically below the separated $\text{NH}_2 + \text{O}$ asymptote. Furthermore, all product channels are exothermic except for $\text{HON} + \text{H}$ (R4), which is slightly endothermic by 0.16 kcal/mol, with the $\text{NO} + \text{H}_2$ (R3) channel being the most exothermic at -82.63 kcal/mol.

The accuracy of the present PIP-NN PES is further corroborated by the minimum energy paths (MEPs) along the reaction coordinate for key transition states, as shown in Figure 4. The close alignment between the PES-derived MEPs and direct *ab initio* calculations confirms the high fidelity of the fitted surface. In addition, a two-dimensional potential energy contour plot was generated for the NH_2O system by fixing NH_2 at its equilibrium geometry and scanning the O atom across the NH_2 plane. Together with the excellent reproduction of stationary point properties, these results demonstrate that the PES faithfully captures the high-level *ab initio* data across the configuration space critical to the reaction dynamics.

B. Thermal Rate Coefficients and Branching Ratios

Based on the newly constructed $\text{NH}_2\text{O}(^2A')$ PES, QCT calculations were performed to investigate the kinetics of the $\text{NH}_2 + \text{O}$ reaction at temperatures of 200, 298, 500, 700, 1000, 1500, 2000, and 2500 K. Approximately 10^5 - 10^6 trajectories were run at each temperature, with statistical uncertainties kept below 0.47%. The total energy was conserved within 10^{-4} kcal/mol for the vast majority of trajectories, confirming the numerical smoothness and stability of the PES during dynamical integration.

Total thermal rate constants obtained from QCT simulations over the temperature range 200-2500 K are listed in Table IV and displayed in Figure 6, alongside available experimental data¹²⁻¹⁴ and earlier theoretical predictions^{22, 32}. Experimental measurements are limited and largely concentrated between 200 and 500 K. Meanwhile, the two existing theoretical studies show markedly different temperature dependencies. Specifically, the rate constants of Sumathi *et al.*²² rise below 500 K and fall at higher temperatures, while those of Klippenstein *et al.*³² decrease below 800 K and increase above this point. In contrast, the present total rate constants calculated on the new PIP-NN PES exhibit a monotonic decrease with increasing temperature, which is characteristic of a barrierless association-dominated reaction. Our computed rate constants of $1.63 \times 10^{-10} \text{ cm}^3 \cdot \text{molecule}^{-1} \cdot \text{s}^{-1}$ at 298 K and $1.04 \times 10^{-10} \text{ cm}^3 \cdot \text{molecule}^{-1} \cdot \text{s}^{-1}$ at 500 K are in excellent agreement with the experimental measurements reported by Inomata and Washida.¹⁴ This close agreement under well-characterized conditions validates the current theoretical framework and justifies its application to predict kinetics at higher combustion-relevant temperatures, where experimental data remain limited.

The temperature-dependent thermal rate constants for the four product channels of the $\text{NH}_2 + \text{O}$ reaction are provided in Table IV and compared with earlier experimental¹²⁻¹⁴ and theoretical^{20-22, 32, 52, 53} results in Figure 7. Notably, in Figure 7(a), the calculated rate constants for the $\text{HNO} +$

H channel at low temperature (<500 K) closely match the experimental data of Inomata and Washida.¹⁴ The corresponding product branching ratios across the studied temperature range (200–2500 K) are summarized in Table V. Over the entire temperature range, the HNO + H channel remains dominant, accounting for 47-70% of the total yield. The NH + OH channel represents a significant secondary pathway (15-40%), while the NO + H₂ channel contributes 10-15%. The HON + H channel remains negligible throughout, never exceeding 3% of the total product yield. Overall, the branching ratios exhibit only moderate temperature dependence. Specifically, the HNO + H and NO + H₂ channels gradually decrease from 70.30% and 14.36% at 200 K to 47% and 10.69% at 2500 K, respectively, whereas the NH + OH and HON + H channels increase from 15.00% and 0.59% to 38.97% and 2.83% over the same range. At low temperature, the reaction is strongly dominated by the HNO + H channel, with the NO + H₂ and NH + OH channels sharing most of the remaining yield. At elevated temperatures, although HNO + H remains the primary channel, the NH + OH pathway grows substantially and approaches it in contribution.

IV. Conclusions

In this work, we have constructed a global full-dimensional potential energy surface for the ground doublet state of the NH₂ + O reaction based on approximately 62,000 high-level *ab initio* points computed at the MRCI-F12/cc-pVTZ-F12 level of theory. The PES, developed using the PIP-NN approach, demonstrates high fidelity in reproducing stationary points, reaction pathways, and reaction energetics across all accessible product channels. Extensive QCT calculations on this PES have yielded thermal rate constants and product branching ratios over a broad temperature range (200-2500 K) providing a first-principles kinetic dataset for this system under combustion-relevant conditions. Our results confirm the dominance of the HNO + H channel and the growing importance of the NH + OH channel as temperature rises, along with a

non-negligible, temperature-insensitive contribution from the $\text{NO} + \text{H}_2$ channel. The theoretically validated rate predictions for the $\text{NH}_2 + \text{O}$ reaction are expected to significantly improve the predictive accuracy of simulations concerning NH_3 ignition and oxidation processes. The kinetics data and mechanistic insights presented here are therefore critical for refining detailed kinetic models of ammonia combustion.

Acknowledgements: This work was supported by the National Natural Science Foundation of China (Grant No. 22503046 to J.Z. and Grant No. 12274229 to W.H.).

Data availability statement: The data that support the findings of this study are available from the corresponding author upon reasonable request.

TABLE I. M diagnostics of all stationary points on the $\text{NH}_2\text{O}(\ ^2A')$ PES.

Species	M diagnostic	Species	M diagnostic
$\text{NH}_2(\ ^2B_1) + \text{O}(\ ^3P)$	0.679	$\text{HNO}(\ ^1A'') + \text{H}$	0.617
$\text{NH}(\ ^3\Sigma^-) + \text{OH}(\ ^2\Pi)$	0.385	$\text{NO}(\ ^2\Pi) + \text{H}_2(\ ^1\Sigma_g^+)$	0.527
$\text{HON}(\ ^3A'') + \text{H}$	0.326	H_2NO	0.390
<i>trans</i> -HNOH	0.254	<i>cis</i> -HNOH	0.247
TS1	0.437	TS2	0.415
TS3	0.419	TS4	0.578
TS5	0.589		

Table II. Optimized geometries of asymptotes and stationary points for the $\text{NH}_2 + \text{O}$ reaction. Distances and angles are in units of \AA and $^\circ$, respectively.

Species	R_{NH}	$R_{\text{NH}'}$	R_{OH}	R_{NO}	R_{HH}	θ_{HNH}	θ_{HNO}	$\theta_{\text{H}'\text{NO}}$	θ_{NOH}	φ_{HNOH}
NH_2	1.024	1.024	/	/	/	102.80	/	/	/	/
HNO	1.211	/	/	1.040	/	/	108.21	/	/	/
HON	/	/	0.968	1.328	/	/	/	/	106.90	
NH	1.036	/	/	/	/	/	/	/	/	/
OH	/	/	0.969	/	/	/	/	/	/	/
NO	/	/	/	1.151	/	/	/	/	/	/
H_2	/	/	/	/	0.743	/	/	/	/	/
H_2NO	1.000	1.006	/	1.272	/	119.23	118.51	118.75	/	158.72
<i>trans</i> - HNOH	1.016	/	0.962	1.371	/	/	105.22	/	103.09	180.00
<i>cis</i> - HNOH	1.018	/	0.964	1.370	/	/	106.00	/	110.70	0.00
TS1	1.019	1.191	/	1.413	/	128.25	106.29	54.41	/	125.74
TS2	1.036	/	0.978	1.410	/	/	102.80	/	105.40	85.40
TS3	1.281	1.281	/	1.236	/	45.37	108.50	108.50	/	47.99
TS4	1.045	/	1.381	1.292	/	121.35	105.41	44.40	/	119.32
TS5	1.061	2.250	/	1.206	2.554	94.03	109.74	135.39	/	118.03

TABLE III. Calculated energies and harmonic vibrational frequencies of all stationary points in the $\text{NH}_2 + \text{O}$ reaction. Energies are given relative to the $\text{NH}_2 + \text{O}$ asymptote, with values in parentheses including ZPE corrections.

Species	Methods	E (kcal/mol)	Harmonic frequencies (cm^{-1})					
			1	2	3	4	5	6
$\text{NH}_2 + \text{O}$	PES ^a	0	1542.55	3374.15	3456.16	\	\	\
	MRCI ^b	0	1553.26	3380.22	3474.87	\	\	\
	CCSD(T) ^c	0	1545.13	3361.50	3455.10	\	\	\
	Expt. ^d	0	1497.33	3219.47	3325.00	\	\	\
$\text{HNO} + \text{H}$	PES ^a	-23.13(-26.09)	1572.04	1752.26	2952.34	\	\	\
	MRCI ^b	-22.98(-26.06)	1558.48	1615.60	3127.47	\	\	\
	CCSD(T) ^c	-22.49(-23.48)	1547.39	1605.42	2956.62	\	\	\
	Expt. ^d	(-26.24 ± 0.05)	1500.82	1565.33	2684.00	\	\	\
$\text{NH} + \text{OH}$	PES ^a	-7.40(-9.36)	3282.22	3768.17	\	\	\	\
	MRCI ^b	-7.28(-9.26)	3284.16	3752.66	\	\	\	\
	CCSD(T) ^c	-7.61(-9.18)	3265.72	3719.69	\	\	\	\
	Expt. ^d	(-9.50 ± 0.07)	3282.23	3737.74	\	\	\	\
$\text{NO} + \text{H}_2$	PES ^a	-79.64(-82.63)	1902.25	4353.29	\	\	\	\
	MRCI ^b	-79.25(-82.49)	1911.21	4382.90	\	\	\	\
	CCSD(T) ^c	-78.84(-79.58)	2116.07	4396.76	\	\	\	\
	Expt. ^d	(-82.49 ± 0.04)	1904.20	4401.21	\	\	\	\
$\text{HON} + \text{H}$	PES ^a	3.44(0.16)	1097.17	1215.88	3722.90	\	\	\
	MRCI ^b	3.35(0.07)	1132.42	1253.02	3726.23	\	\	\
	CCSD(T) ^c	3.12(1.33)	1285.44	1473.64	3314.05	\	\	\
	Expt. ^d	(-0.43 ± 0.21)	\	\	\	\	\	\
H_2NO	PES ^a	-90.28(-85.58)	145.39	1275.93	1410.45	1748.99	3498.46	3647.73
	MRCI ^b	-89.43(-84.42)	386.64	1297.23	1372.84	1681.63	3485.97	3688.66
<i>trans</i> -HNOH	PES ^a	-83.74(-78.62)	715.17	1104.54	1245.97	1540.74	3388.29	3833.69
	MRCI ^b	-83.32(-78.08)	750.96	1099.30	1289.44	1600.40	3522.74	3808.60
<i>cis</i> -HNOH	PES ^a	-77.78(-73.40)	527.92	1095.81	1329.92	1479.07	3353.69	3765.78
	MRCI ^b	-77.66(-72.81)	577.73	1087.57	1355.69	1537.65	3472.28	3767.58
TS1	PES ^a	-36.99(-34.09)	2044.23i	770.01	1003.49	1378.05	2628.98	3436.14
	MRCI ^b	-36.75(-35.54)	2146.75i	804.60	1023.85	1372.77	2592.09	3463.61
TS2	PES ^a	-69.95(-66.68)	951.68i	985.55	1228.99	1450.13	3310.88	3800.00
	MRCI ^b	-68.61(-65.48)	863.83i	971.16	1272.98	1479.33	3271.93	3597.58
TS3	PES ^a	-23.55(-25.72)	1526.02i	540.89	1131.90	1216.22	1473.63	2490.76
	MRCI ^b	-22.74(-25.00)	1784.82i	834.33	1136.29	1144.81	1428.79	2278.38
TS4	PES ^a	-18.19(-18.77)	1230.90i	288.02	465.29	1420.28	1552.34	3021.24
	MRCI ^b	-16.37(-18.28)	988.74i	343.07	496.67	1412.76	1589.68	3229.13
TS5	PES ^a	-22.61(-24.95)	461.46i	245.12	465.66	1443.88	1568.10	2944.90
	MRCI ^b	-22.15(-24.54)	333.65i	228.63	431.33	1578.88	1600.79	2898.88

^a Fitted PES, this work; ^b MRCI-F12/cc-pVTZ-F12, this work; ^c UCCSD(T)-F12/cc-pVTZ-F12;

^d Ref.⁵¹.

Table IV. Rate coefficients ($\text{cm}^3 \cdot \text{molecule}^{-1} \cdot \text{s}^{-1}$) for the $\text{NH}_2 + \text{O}$ reaction obtained from QCT calculations. k is the total rate coefficient. $k_{\text{HNO}+\text{H}}$, $k_{\text{NH}+\text{OH}}$, $k_{\text{NO}+\text{H}_2}$, and $k_{\text{HON}+\text{H}}$ are rate coefficients for the $\text{HNO} + \text{H}$, $\text{NH} + \text{OH}$, $\text{NO} + \text{H}_2$ and $\text{HON} + \text{H}$ channels, respectively.

T / K	k	$k_{\text{HNO}+\text{H}}$	$k_{\text{NH}+\text{OH}}$	$k_{\text{NO}+\text{H}_2}$	$k_{\text{HON}+\text{H}}$
200	2.02×10^{-10}	1.42×10^{-10}	3.03×10^{-11}	2.90×10^{-11}	1.19×10^{-12}
298	1.63×10^{-10}	1.13×10^{-10}	2.58×10^{-11}	2.29×10^{-11}	9.84×10^{-13}
500	1.04×10^{-10}	7.11×10^{-11}	1.84×10^{-11}	1.40×10^{-11}	7.32×10^{-13}
700	7.58×10^{-11}	5.02×10^{-11}	1.51×10^{-11}	9.77×10^{-12}	6.61×10^{-13}
1000	5.50×10^{-11}	3.46×10^{-11}	1.28×10^{-11}	6.87×10^{-12}	6.92×10^{-13}
1500	4.10×10^{-11}	2.36×10^{-11}	1.20×10^{-11}	4.75×10^{-12}	7.19×10^{-13}
2000	3.52×10^{-11}	1.83×10^{-11}	1.21×10^{-11}	3.90×10^{-12}	8.68×10^{-13}
2500	3.31×10^{-11}	1.57×10^{-11}	1.29×10^{-11}	3.54×10^{-12}	9.38×10^{-13}

Table V. Product branching ratios for the $\text{NH}_2 + \text{O}$ reaction.

T / K	$\text{HNO} + \text{H}$	$\text{NH} + \text{OH}$	$\text{NO} + \text{H}_2$	$\text{HON} + \text{H}$
200	70.30%	15.00%	14.36%	0.59%
298	69.33%	15.83%	14.05%	0.60%
500	68.37%	17.69%	13.46%	0.70%
700	66.23%	19.92%	12.89%	0.87%
1000	62.91%	23.27%	12.49%	1.26%
1500	57.56%	29.27%	11.59%	1.75%
2000	51.99%	34.38%	11.08%	2.47%
2500	47.43%	38.97%	10.69%	2.83%

References

- ¹ A. Valera-Medina, H. Xiao, M. Owen-Jones, W. I. F. David, and P. J. Bowen, "Ammonia for power," *Prog. Energy Combust. Sci.* **69**, 63–102 (2018).
- ² H. Kobayashi, A. Hayakawa, K. K. A. Somarathne, and E. C. Okafor, "Science and technology of ammonia combustion," *Proc. Combust. Inst.* **37**, 109–133 (2019).
- ³ O. Elishav, B. Mosevitzky Lis, E. M. Miller, D. J. Arent, A. Valera-Medina, A. Grinberg Dana, G. E. Shter, and G. S. Grader, "Progress and Prospective of Nitrogen-Based Alternative Fuels," *Chem. Rev.* **120**, 5352–5436 (2020).
- ⁴ A. Valera-Medina, F. Amer-Hatem, A. K. Azad, I. C. Dedoussi, M. de Joannon, R. X. Fernandes, P. Glarborg, H. Hashemi, X. He, S. Mashruk, J. McGowan, C. Mounaim-Rouselle, A. Ortiz-Prado, A. Ortiz-Valera, I. Rossetti, B. Shu, M. Yehia, H. Xiao, and M. Costa, "Review on Ammonia as a Potential Fuel: From Synthesis to Economics," *Energy Fuels* **35**, 6964–7029 (2021).
- ⁵ K. Lianwei, P. Weiguo, Z. Jiakai, W. Wenhuan, and T. Congwei, "A review on ammonia blends combustion for industrial applications," *Fuel* **332**, 126150 (2023).
- ⁶ N. Hisashi, H. Susumu, and T. Takuya, "Kinetic modeling of ammonia/air weak flames in a micro flow reactor with a controlled temperature profile," *Combust. Flame* **185**, 16–27 (2017).
- ⁷ M. Bowen, Z. Xiaoyuan, M. Siyuan, C. Mingli, G. Hanwen, C. Zhihao, and L. Yuyang, "Experimental and kinetic modeling investigation on the laminar flame propagation of ammonia under oxygen enrichment and elevated pressure conditions," *Combust. Flame* **210**, 236–246 (2019).
- ⁸ H. Xinlu, W. Zhihua, H. Yong, Z. Yanqun, and C. Kefa, "Experimental and kinetic modeling study of laminar burning velocities of NH₃/syngas/air premixed flames," *Combust. Flame* **213**, 1–13 (2020).
- ⁹ A. Stagni, C. Cavallotti, S. Arunthanayothin, Y. Song, O. Herbinet, F. Battin-Leclerc, and T. Faravelli, "An experimental, theoretical and kinetic-modeling study of the gas-phase oxidation of ammonia," *React. Chem. Eng.* **5**, 696–711 (2020).
- ¹⁰ H. Xinlu, L. Marco Lubrano, and K. Alexander A., "An experimental and kinetic modeling study on the laminar burning velocity of NH₃+N₂O⁺ air flames," *Combust. Flame* **228**, 13–28 (2021).
- ¹¹ M. Gehring, K. Hoyermann, H. Schacke, and J. Wolfrum, "Direct studies of some elementary steps for the formation and destruction of nitric oxide in the H-N-O system," *Symp. (Int.) Combust.* **14**, 99–105 (1973).
- ¹² P. Dransfeld, W. Hack, H. Kurzke, F. Temps, and H. G. Wagner, "Direct studies of elementary reactions of NH₂-radicals in the gas phase," *Chem. Phys. Lett.* **20**, 655–663 (1985).
- ¹³ J. D. Adamson, S. K. Farhat, C. L. Morter, G. P. Glass, R. F. Curl, and L. F. Phillips, "The Reaction of NH₂ with O," *J. Phys. Chem.* **98**, 5665–5669 (1994).
- ¹⁴ S. Inomata, and N. Washida, "Rate Constants for the Reactions of NH₂ and HNO with Atomic Oxygen at Temperatures between 242 and 473 K," *J. Phys. Chem. A* **103**, 5023–5031 (1999).
- ¹⁵ D. Patel-Misra, D. G. Sauder, and P. J. Dagdigian, "Internal state distribution of OD produced from the O(³P)+ND₂ reaction," *J. Chem. Phys.* **95**, 955–962 (1991).
- ¹⁶ D. Patel-Misra, and P. J. Dagdigian, "Dynamics of the O(³P)+NH₂ reaction: the HNO + H product channel," *Chem. Phys. Lett.* **185**, 387–392 (1991).
- ¹⁷ S. P. Walch, "Theoretical characterization of the reaction NH₂+O→products," *J. Chem. Phys.* **99**, 3804–3808 (1993).

- ¹⁸ D. L. Yang, M. L. Koszykowski, and J. L. Durant, Jr., "The reaction of $\text{NH}_2(X^2B_1)$ with O (X^3P): A theoretical study employing Gaussian 2 theory," *J. Chem. Phys.* **101**, 1361–1368 (1994).
- ¹⁹ M. Wolf, D. L. Yang, and J. L. Durant, "Kinetic studies of NH_x radical reactions," *J. Photochem. Photobiol. A Chem.* **80**, 85–93 (1994).
- ²⁰ J. Bozzelli, and A. Dean, "Energized complex quantum Rice-Ramsperger-Kassel analysis of reactions of NH_2 , O_2 , and O atoms," *J. Phys. Chem.* **93**, 1058–1065 (1989).
- ²¹ X. Duan, and M. Page, "*Ab initio* variational transition state theory calculations for the $\text{O}+\text{NH}_2$ hydrogen abstraction reaction on the $^4A'$ and $^4A''$ potential energy surfaces," *J. Chem. Phys.* **102**, 6121–6127 (1995).
- ²² R. Sumathi, D. Sengupta, and M. T. Nguyen, "Theoretical Study of the $\text{H}_2 + \text{NO}$ and Related Reactions of $[\text{H}_2\text{NO}]$ Isomers," *J. Phys. Chem. A* **102**, 3175–3183 (1998).
- ²³ M. R. Soto, and M. Page, "*Ab initio* variational transition-state-theory reaction-rate calculations for the gas-phase reaction $\text{H}+\text{HNO}\rightarrow\text{H}_2+\text{NO}$," *J. Chem. Phys.* **97**, 7287–7296 (1992).
- ²⁴ M. Page, and M. R. Soto, "Radical addition to HNO. *Ab initio* reaction path and variational transition state theory calculations for $\text{H}+\text{HNO}\rightarrow\text{H}_2\text{NO}$ and $\text{H}+\text{HNO}\rightarrow\text{HNOH}$," *J. Chem. Phys.* **99**, 7709–7717 (1993).
- ²⁵ H. M. T. Nguyen, S. Zhang, J. Peeters, T. N. Truong, and M. T. Nguyen, "Direct ab initio dynamics studies of the reactions of HNO with H and OH radicals," *Chem. Phys. Lett.* **388**, 94–99 (2004).
- ²⁶ E. Vessally, S. Ebrahimi, M. Goodarzi, and A. Seif, "Insight into detailed mechanism of the atmospheric reaction of imidogen with hydroxyl: a computational study," *Struct. Chem.* **25**, 169–175 (2014).
- ²⁷ S. S. Asemani, and S. H. Mousavipour, "Dynamics of imidogen reaction with hydroxyl radical: a theoretical approach," *J. Iran. Chem. Soc.* **17**, 1987–2000 (2020).
- ²⁸ R. Sharafadini, and S. Ramazani, "Dynamic and Kinetic Parameters and Energy Exchanges of Particles in Reaction of $\text{NH} + \text{OH}$ and Deuterated Analogues on an Interpolated Potential Energy Surface," *ChemistrySelect* **5**, 3518–3528 (2020).
- ²⁹ Y. Kurosaki, and T. Takayanagi, "*Ab initio* molecular orbital study of potential energy surface for the $\text{H}_2\text{NO}(^2B_1)\rightarrow\text{NO}(^2\Pi)+\text{H}_2$ reaction," *J. Mol. Struct.: THEOCHEM* **507**, 119–126 (2000).
- ³⁰ Z. Homayoon, and J. M. Bowman, "A Global Potential Energy Surface Describing the $\text{N}(^2D) + \text{H}_2\text{O}$ Reaction and a Quasiclassical Trajectory Study of the Reaction to $\text{NH} + \text{OH}$," *J. Phys. Chem. A* **118**, 545–553 (2014).
- ³¹ M. Isegawa, F. Liu, S. Maeda, and K. Morokuma, "Complete active space second order perturbation theory (CASPT2) study of $\text{N}(^2D) + \text{H}_2\text{O}$ reaction paths on D_1 and D_0 potential energy surfaces: Direct and roaming pathways," *J. Chem. Phys.* **141**(2014).
- ³² S. J. Klippenstein, C. R. Mulvihill, and P. Glarborg, "Theoretical Kinetics Predictions for Reactions on the NH_2O Potential Energy Surface," *J. Phys. Chem. A* **127**, 8650–8662 (2023).
- ³³ P. J. Knowles, and H.-J. Werner, "An efficient method for the evaluation of coupling coefficients in configuration interaction calculations," *Chem. Phys. Lett.* **145**, 514–522 (1988).
- ³⁴ T. Shiozaki, G. Knizia, and H.-J. Werner, "Explicitly correlated multireference configuration interaction: MRCI-F12," *J. Chem. Phys.* **134**(2011).
- ³⁵ J. Li, B. Jiang, and H. Guo, "Permutation invariant polynomial neural network approach to fitting potential energy surfaces. II. Four-atom systems," *J. Chem. Phys.* **139**, 204103 (2013).

- ³⁶ B. Jiang, and H. Guo, "Permutation invariant polynomial neural network approach to fitting potential energy surfaces," J. Chem. Phys. **139**, 054112 (2013).
- ³⁷ M. P. Deskevich, D. J. Nesbitt, and H.-J. Werner, "Dynamically weighted multiconfiguration self-consistent field: Multistate calculations for $F+H_2O \rightarrow HF+OH$ reaction paths," J. Chem. Phys. **120**, 7281–7289 (2004).
- ³⁸ R. Dawes, A. W. Jasper, C. Tao, C. Richmond, C. Mukarakate, S. H. Kable, and S. A. Reid, "Theoretical and Experimental Spectroscopy of the S_2 State of CHF and CDF: Dynamically Weighted Multireference Configuration Interaction Calculations for High-Lying Electronic States," J. Phys. Chem. Lett. **1**, 641–646 (2010).
- ³⁹ S. R. Langhoff, and E. R. Davidson, "Configuration interaction calculations on the nitrogen molecule," Int. J. Quantum Chem. **8**, 61–72 (1974).
- ⁴⁰ K. A. Peterson, T. B. Adler, and H.-J. Werner, "Systematically convergent basis sets for explicitly correlated wavefunctions: The atoms H, He, B–Ne, and Al–Ar," J. Chem. Phys. **128**, 084102 (2008).
- ⁴¹ K. Gerald, T. B. Adler, and W. Hans-Joachim, "Simplified CCSD(T)-F12 methods: theory and benchmarks," J. Chem. Phys. **130**, 221106 (2009).
- ⁴² T. B. Adler, G. Knizia, and H.-J. Werner, "A simple and efficient CCSD(T)-F12 approximation," J. Chem. Phys. **127**, 221106 (2007).
- ⁴³ H.-J. Werner, P. J. Knowles, G. Knizia, F. R. Manby, and M. Schütz, "Molpro: a general-purpose quantum chemistry program package," WIREs Comput. Mol. Sci. **2**, 242–253 (2012).
- ⁴⁴ B. Jiang, J. Li, and H. Guo, "Potential energy surfaces from high fidelity fitting of ab initio points: the permutation invariant polynomial - neural network approach," Int. Rev. Phys. Chem. **35**, 479–506 (2016).
- ⁴⁵ B. J. Braams, and J. M. Bowman, "Permutationally invariant potential energy surfaces in high dimensionality," Int. Rev. Phys. Chem. **28**, 577–606 (2009).
- ⁴⁶ M. T. Hagan, and M. B. Menhaj, "Training feedforward networks with the Marquardt algorithm," IEEE Trans. Neural Netw. **5**, 989–993 (1994).
- ⁴⁷ L. M. Raff, R. Komanduri, M. Hagan, and S. T. S. Bukkapatnam, *Neural Networks in Chemical Reaction Dynamics* (Oxford University Press, 2012),
- ⁴⁸ W. L. Hase, R. J. Duchovic, X. Hu, A. Komornicki, K. F. Lim, D.-h. Lu, G. H. Peslherbe, K. N. Swamy, S. Linde, and A. Varandas, "A general chemical dynamics computer program," Quantum Chem. Program Exch. Bull **16**, 671 (1996).
- ⁴⁹ Y. Guo, D. L. Thompson, and T. D. Sewell, "Analysis of the zero-point energy problem in classical trajectory simulations," J. Chem. Phys. **104**, 576–582 (1996).
- ⁵⁰ D. G. Truhlar, "Multiple potential energy surfaces for reactions of species in degenerate electronic states," J. Chem. Phys. **56**, 3189–3190 (1972).
- ⁵¹ K. Huber, *Molecular spectra and molecular structure: IV. Constants of diatomic molecules* (Springer Science & Business Media, 2013),
- ⁵² J. A. Miller, M. D. Smooke, R. M. Green, and R. J. Kee, "Kinetic Modeling of the Oxidation of Ammonia in Flames," Combust. Sci. Technol. **34**, 149–176 (1983).
- ⁵³ A. M. Dean, and J. W. Bozzelli, in *Gas-phase combustion chemistry* (Springer, 2000), pp. 125–341.
- ⁵⁴ S. J. Klippenstein, L. B. Harding, B. Ruscic, R. Sivaramakrishnan, N. K. Srinivasan, M. C. Su, and J. V. Michael, "Thermal decomposition of NH_2OH and subsequent reactions: *Ab initio* transition state theory and reflected shock tube experiments," J. Phys. Chem. A **113**, 10241–10259 (2009).

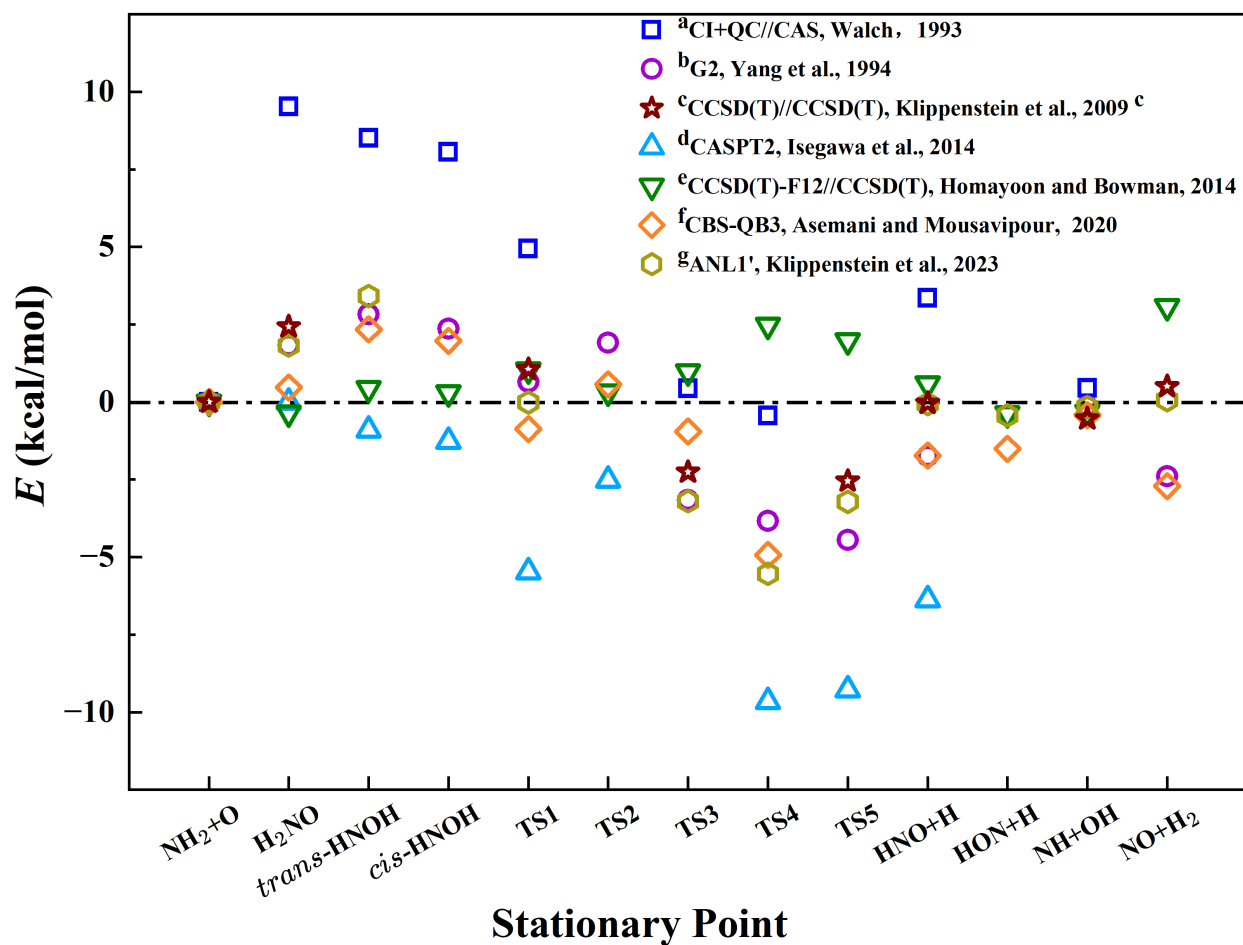


Fig. 1. Deviations of literature stationary point energies benchmarked against the present MRCI-F12/VTZ-F12 calculations. Note: ^aMRCI+QC/TZ//CAS/DZ calculations from ref. ¹⁷. ^bG2 calculations from ref. ¹⁸. ^cCCSD(T)/CBS//CCSD(T)/ATZ calculations from ref. ⁵⁴. ^dCASPT2(13e,10o)/TZ calculations from ref. ³¹. ^eCCSD(T)-F12/AQZ//CCSD(T)/311+G(d,p) calculations with UMP2/6-311+G(d,p) ZPE corrections from ref. ³⁰. ^fCBS-QB3 calculations from ref. ²⁷. ^gANL1//CCSD(T)-F12/cc-pVQ,T-F12 level from ref. ³².

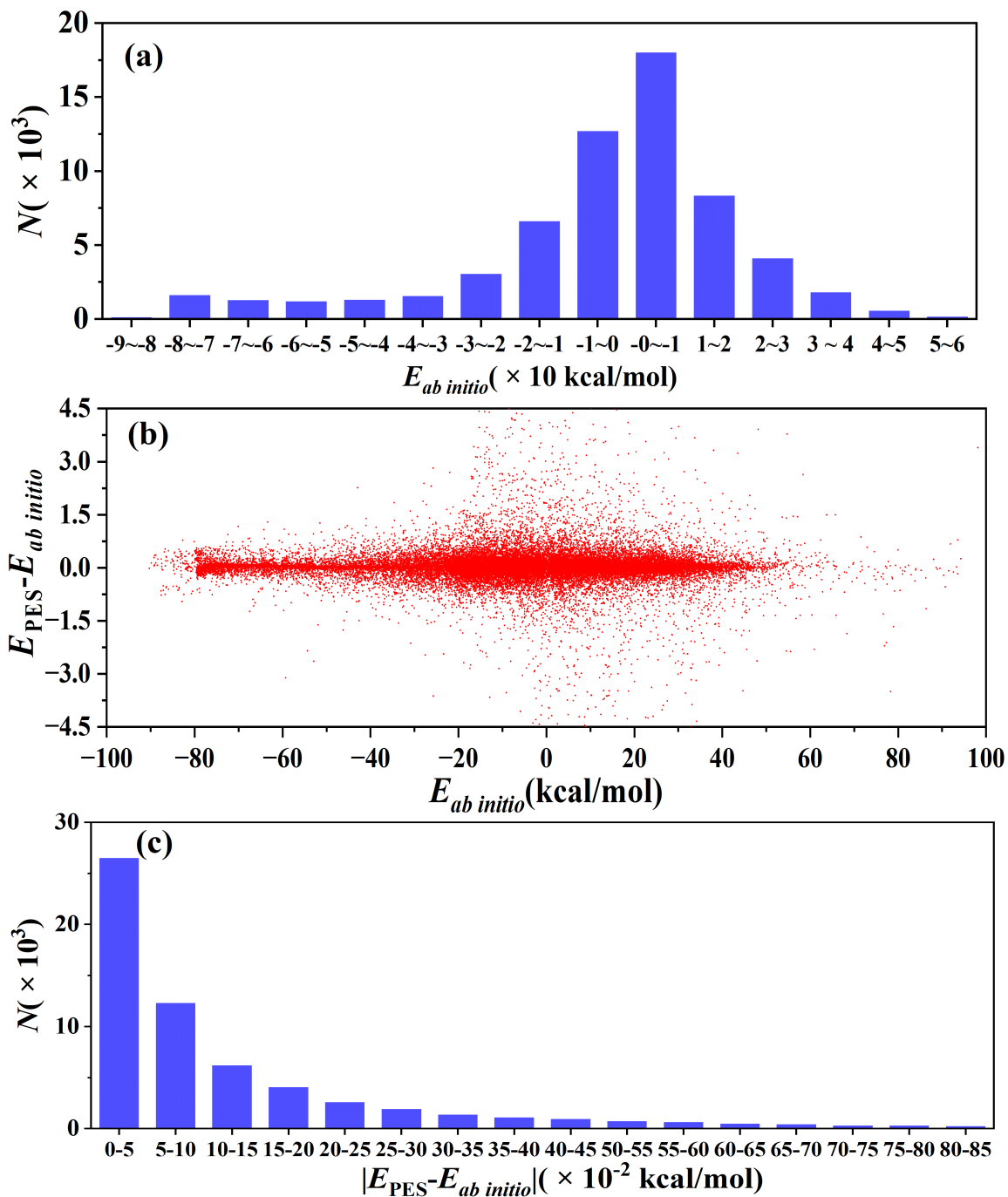


Fig. 2. (a) Distribution of *ab initio* points for the PIP-NN PES. (b) Fitting errors as a function of the *ab initio* energy. (c) Distribution of the fitting errors for the selected points. The values of the potential energy are relative to the $\text{NH}_2 + \text{O}$ reaction. All energies are in unit of kcal/mol.

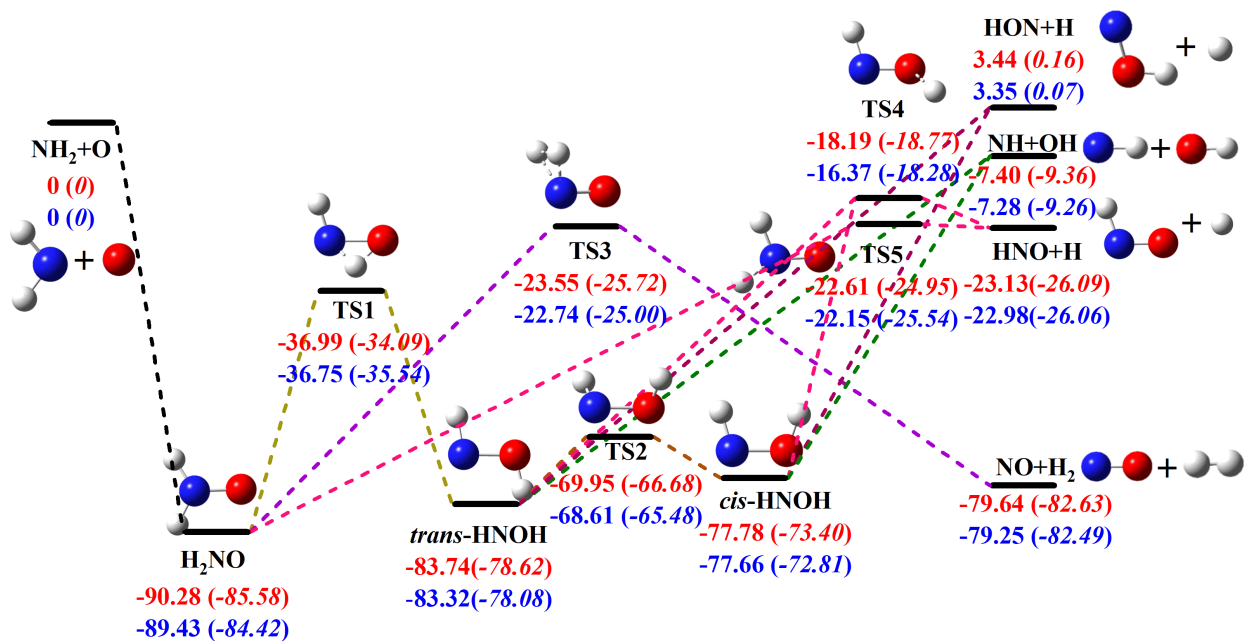


Fig. 3. Schematic reaction pathways for the $\text{NH}_2 + \text{O}$ reaction. Stationary-point energies are shown both without (upright) and with (italic) ZPE corrections, obtained from the present PES (red) and from reference ab initio calculations (blue). All values are given in kcal/mol relative to the reactants.

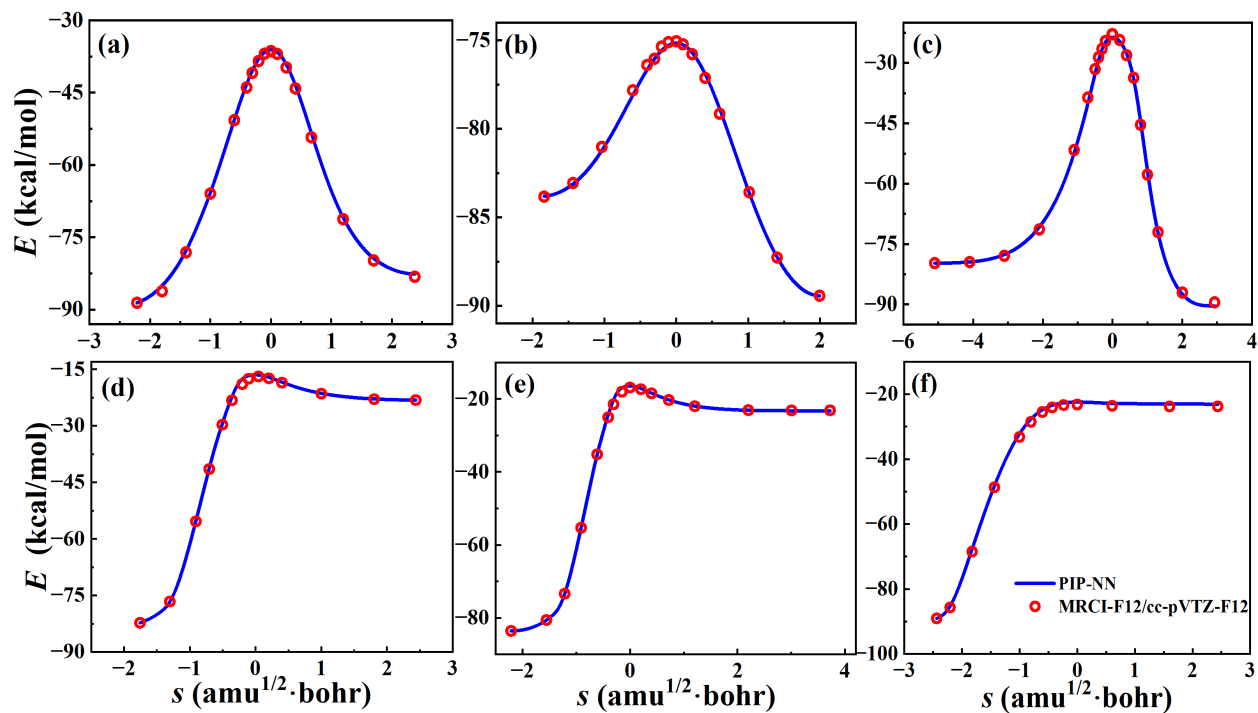


Fig. 4. Minimum energy paths (MEPs) along reaction coordinate for key processes: (a) $\text{H}_2\text{NO} \rightarrow \text{TS1} \rightarrow \text{trans-HNOH}$, (b) $\text{trans-HNOH} \rightarrow \text{TS2} \rightarrow \text{cis-HNOH}$, (c) $\text{H}_2\text{NO} \rightarrow \text{TS3} \rightarrow \text{NO} + \text{H}_2$, (d) $\text{trans-HNOH} \rightarrow \text{TS4} \rightarrow \text{HNO} + \text{H}$, (e) $\text{cis-HNOH} \rightarrow \text{TS4} \rightarrow \text{HNO} + \text{H}$, and (f) $\text{H}_2\text{NO} \rightarrow \text{TS5} \rightarrow \text{HNO} + \text{H}$. Solid lines represent MEPs traced on the fitted PES, while symbols denote the benchmark *ab initio* energy points.

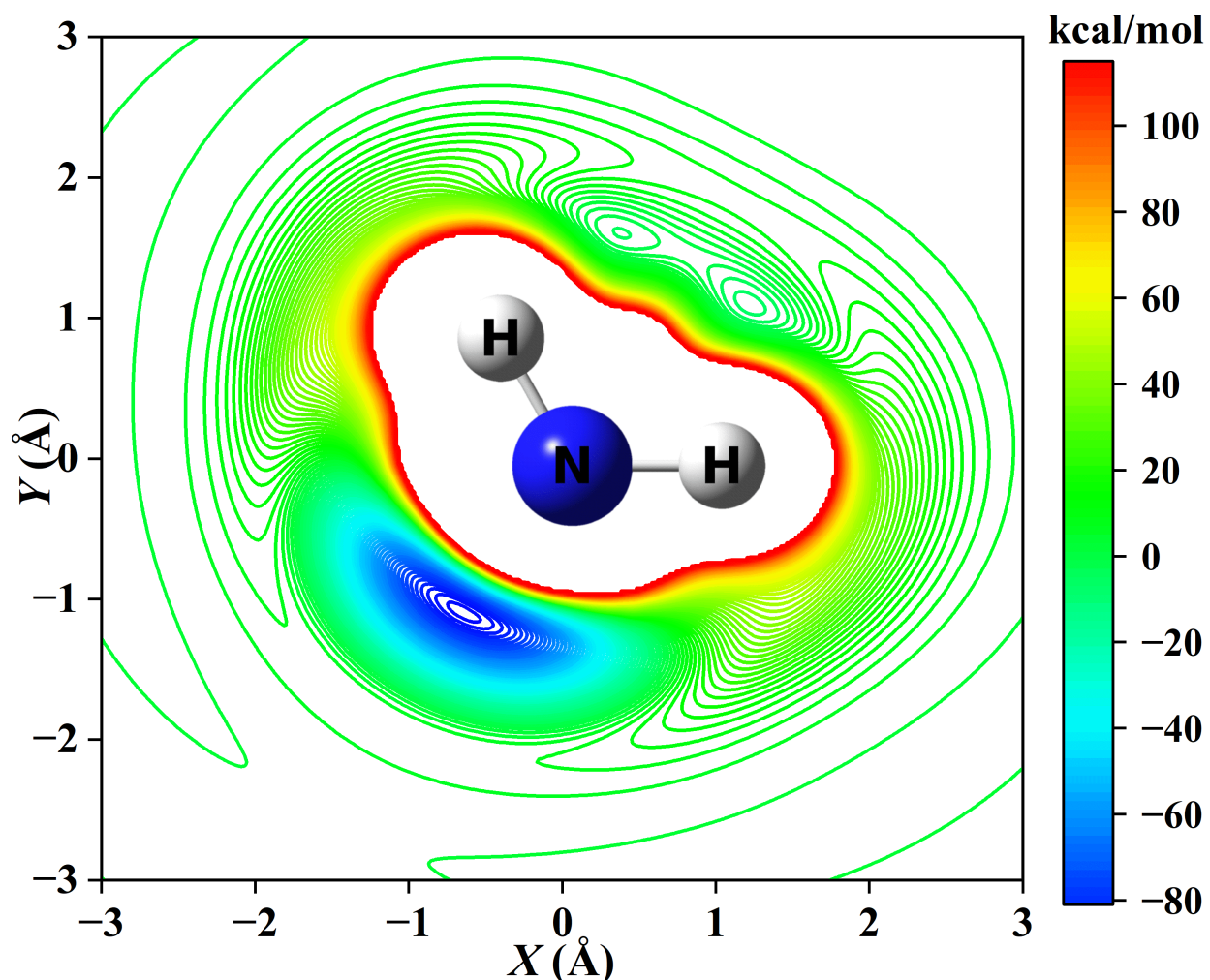


Fig. 5. Two-dimensional potential energy contour plot of the NH₂O system by fixing the NH₂ at its equilibrium geometry and scanning the O atom across the NH₂ plane. Energies are in kcal/mol relative to the NH₂ + O asymptote with contour interval of 2 kcal/mol.

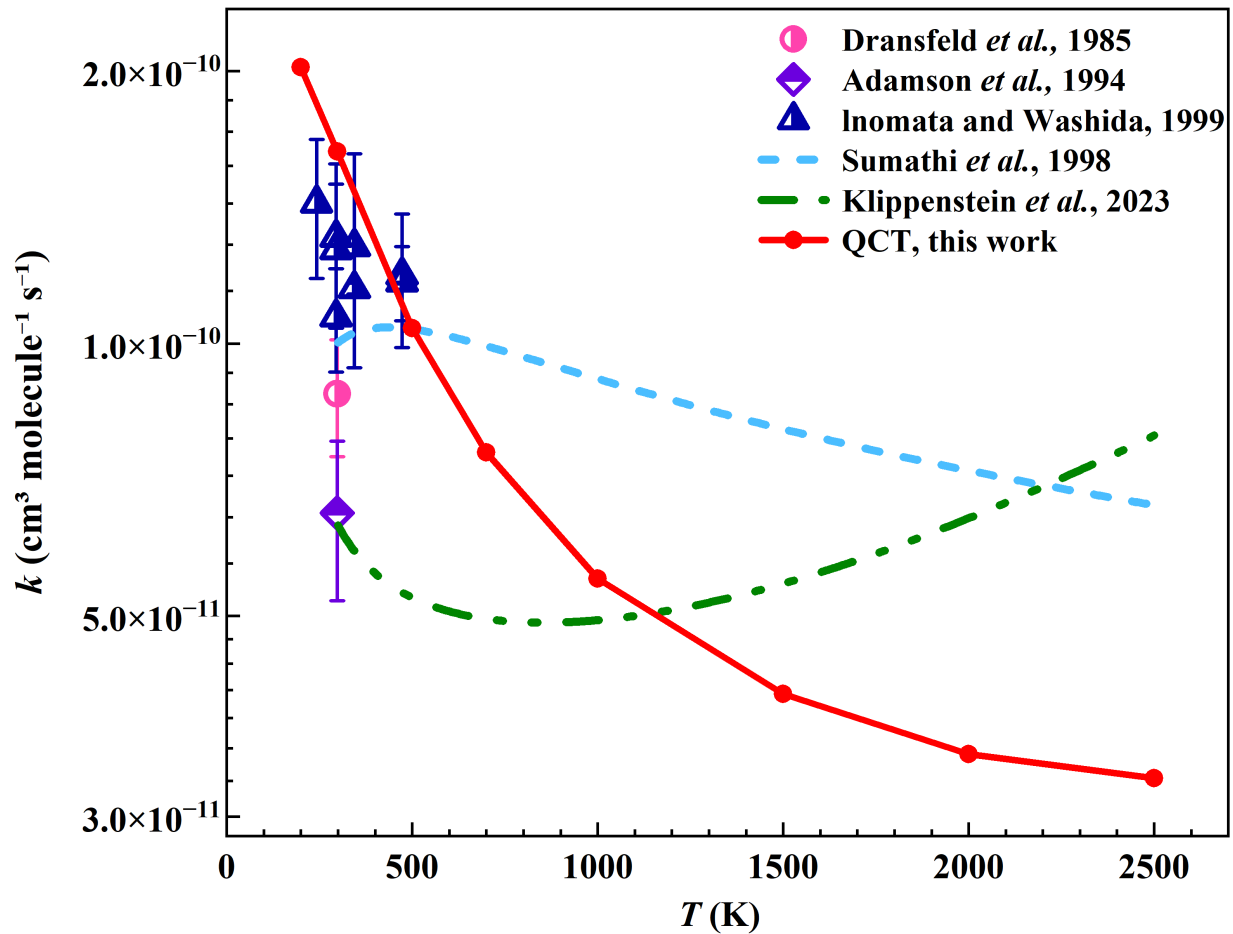


Fig. 6. Temperature dependence of the total thermal rate coefficients for the $\text{NH}_2 + \text{O}$ reaction, alongside available experimental¹²⁻¹⁴ and theoretical^{22, 32} data from literatures.

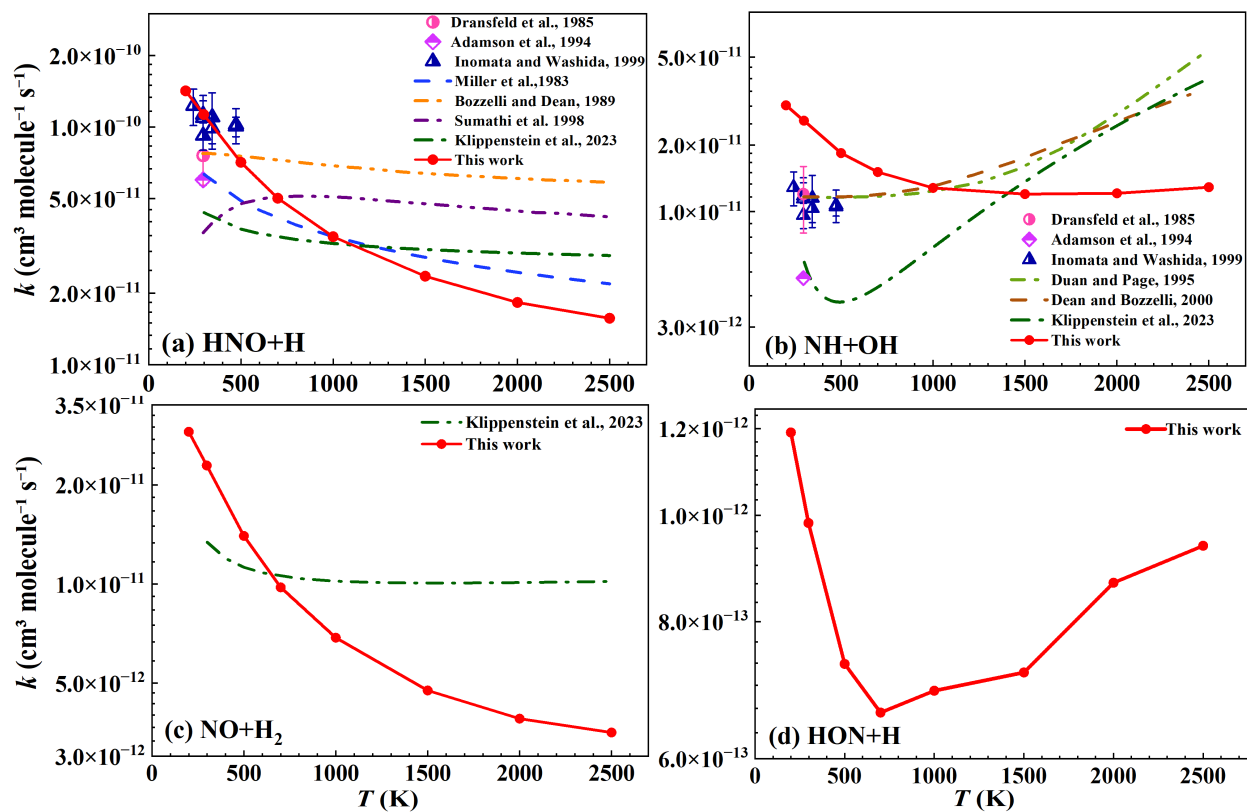


Fig. 7. Temperature dependence of the thermal rate coefficients for the four product channels of the $\text{NH}_2 + \text{O}$ reaction, alongside available experimental¹²⁻¹⁴ and theoretical^{20-22, 32, 52, 53} data from literatures.